RESEARCH ARTICLE | NOVEMBER 03 2025

# Fundamental bounds of wavefront shaping of spatially entangled photons •

Special Collection: Light Dynamics in Active and Passive Randomized Media

Ronen Shekel (10); Sébastien M. Popoff (10); Yaron Bromberg (12)



APL Photonics 10, 110801 (2025) https://doi.org/10.1063/5.0278947





# Articles You May Be Interested In

Rapid and efficient wavefront correction for spatially entangled photons using symmetrized optimization

API Photonics (September 2025)

Partial immunity of two-photon correlation against wavefront distortion for spatially entangled photons

Shaping single photons through multimode optical fibers using mechanical perturbations

APL Photonics (September 2023)



# Fundamental bounds of wavefront shaping of spatially entangled photons •

Cite as: APL Photon. 10, 110801 (2025); doi: 10.1063/5.0278947

Submitted: 4 May 2025 • Accepted: 13 October 2025 •

**Published Online: 3 November 2025** 











Ronen Shekel,<sup>1</sup> D Sébastien M. Popoff,<sup>2</sup> D and Yaron Bromberg<sup>1,a)</sup> D



# **AFFILIATIONS**

- <sup>1</sup>Racah Institute of Physics, The Hebrew University of Jerusalem, Jerusalem 91904, Israel
- <sup>2</sup>Institut Langevin, ESPCI Paris, PSL University, CNRS, Paris, France

Note: This paper is part of the Special Topic on Light Dynamics in Active and Passive Randomized Media.

a) Author to whom correspondence should be addressed: Yaron.Bromberg@mail.huji.ac.il

#### **ABSTRACT**

Wavefront shaping enables control of classical light through scattering media. Extending these techniques to spatially entangled photons promises new quantum applications, but their fundamental limits, especially when both photons scatter, remain unclear. Here, we theoretically and numerically investigate the enhancement of two-photon correlations in two specific output modes through thick scattering media. We analyze three configurations: shaping one photon after the medium, shaping both photons before the medium, and shaping both photons after the medium. We show that each configuration yields fundamentally different enhancements compared to classical expectations. For a system with N modes, we show that shaping one photon yields the classical enhancement  $\eta \approx (\pi/4)N$ , while shaping both photons before the medium reduces it to  $\eta \approx (\pi/4)^2 N$ . However, in some symmetric detection schemes, when both photons are measured at the same mode, perfect correlations are restored with  $\eta \approx N$ , resembling digital optical phase conjugation. Conversely, shaping both photons after the medium leads to a complex, NP-hard-like optimization problem, yet achieves superior enhancements, up to  $\eta \approx 4.6N$ . These results reveal unique quantum effects in complex media and identify strategies for quantum imaging and communication through scattering environments.

© 2025 Author(s). All article content, except where otherwise noted, is licensed under a Creative Commons Attribution (CC BY) license (https://creativecommons.org/licenses/by/4.0/). https://doi.org/10.1063/5.0278947

# I. INTRODUCTION

When classical light propagates through a complex medium such as white paint or biological tissue, it is scattered, producing a random speckle pattern. In their seminal work,1 Vellekoop and Mosk demonstrated that by shaping the incoming wavefront using a spatial light modulator (SLM), the strong scattering could be overcome, initiating the field of wavefront shaping.<sup>2</sup> Since then, the scope of wavefront shaping has grown considerably, with advances in optimization algorithms, feedback mechanisms, and a variety of shaping modalities.

Wavefront shaping has proven powerful for classical applications, including deep-tissue imaging and optical communications. Its extension to the quantum domain<sup>7</sup> creates new opportunities, particularly for quantum imaging and secure quantum communications. 8-14 In particular, spatially entangled photons produced by spontaneous parametric down-conversion (SPDC) exhibit strong correlations that are also scrambled when propagating through a complex medium, resulting in a two-photon speckle. 15 Over the past decade, experiments have shown that standard wavefront shaping tools can be applied directly to these two-photon correlations.

In quantum communication schemes, one photon of an entangled pair is typically retained at the transmitter while the other is sent through a complex quantum channel. Several works 17-22 have studied this scenario, where only a single photon experiences scattering. Since the classical and quantum light share the same spatial modes, the scattering of classical light, a weak coherent beam, and heralded single photons are all described by the same transmission matrix, and a classical beacon could be used to find optimal phases that restore the correlations. 17–19,22

In quantum imaging and related applications, both photons may propagate through the complex medium. 23-33 In this case, the phases that localize the correlations after the scattering differ from

those that would focus a classical beacon beam,<sup>32</sup> and therefore a classical beacon cannot be used for feedback. One solution is to use the weak two-photon correlations for feedback.<sup>21,26,30,32</sup> Alternatively, several classical feedback strategies have been proposed: (a) measuring the one-photon transmission matrix and inferring the two-photon transmission matrix from it;<sup>23,24</sup> (b) using the pump beam for feedback in the case of thin diffusers;<sup>27,28,34</sup> or (c) employing an advanced wave beacon beam.<sup>31</sup> The fact that a classical beacon scatters differently from the two-photon state implies that the performance bounds of wavefront shaping, derived for classical light,<sup>35</sup> are not directly applicable to this quantum scenario.

In this work, we examine the fundamental limits of restoring the correlations between entangled photons that both propagate through a thick scattering medium. We show, both analytically and numerically, that the optimal enhancement in the quantum case differs from the classical enhancement and depends on several factors, including the relative locations of the two detectors and the plane at which the SLM is positioned. In particular, we show that in certain symmetric scenarios, perfect compensation of scattering is achievable, an effect we interpret as a form of digital optical phase conjugation. We further show that when the SLM is placed after the scattering medium, the optimization problem resembles NP-hard problems. Nevertheless, numerical solutions exhibit superior performance compared to classical shaping. Notably, this includes instances where the optimized coincidence rate at the target modes exceeds the total coincidence rate summed over all modes before shaping. These results are determined by the optimal shaping phases, regardless of the method used to obtain them.

# II. RESULTS

We consider spatially entangled photons generated via spontaneous parametric down-conversion (SPDC).<sup>36</sup> In SPDC, a strong pump beam impinges on a nonlinear crystal, and with some probability, one pump photon is annihilated and two lower-energy photons are created. Depending on the phase-matching conditions of the nonlinear crystal, the generated photon pairs can be entangled in their polarization, spectral, and spatial degrees of freedom. Since this work focuses on spatial wavefront shaping, we simplify the analysis by considering the case where the photons are indistinguishable and share the same polarization (type-I SPDC) and the same frequency (degenerate SPDC). Under these conditions, we examine spatially entangled photons, whose state can be approximated by  $|\Psi_{\rm in}\rangle=\frac{1}{\sqrt{2N}}\sum_{\bf x}\hat{a}_{\bf x}^{\dagger}\hat{a}_{\bf x}^{\dagger}|{\rm vac}\rangle$ , where  $\hat{a}_{\bf x}^{\dagger}$  is the creation operator in the transverse position  $\mathbf{x}$ ,  $|vac\rangle$  denotes the vacuum state, and N is the number of modes in the discretized space. Experimentally, this state is obtained by weakly focusing the pump beam on the nonlinear crystal, operating in the so-called thin crystal regime.<sup>3</sup>

We are interested in a scenario where both photons propagate through a thick scattering sample, operating in the multiple scattering regime, where the sample thickness L is much larger than the transport mean free path  $\ell^*$ . This ensures complete randomization of the transmitted light with no ballistic component. We also assume the photons' wavelength to be much smaller than  $\ell^*$ , keeping us far from the Anderson localization regime. We model the scattering medium by a transmission matrix T, and consider two models for T: (i) A random unitary matrix, which describes, for example,

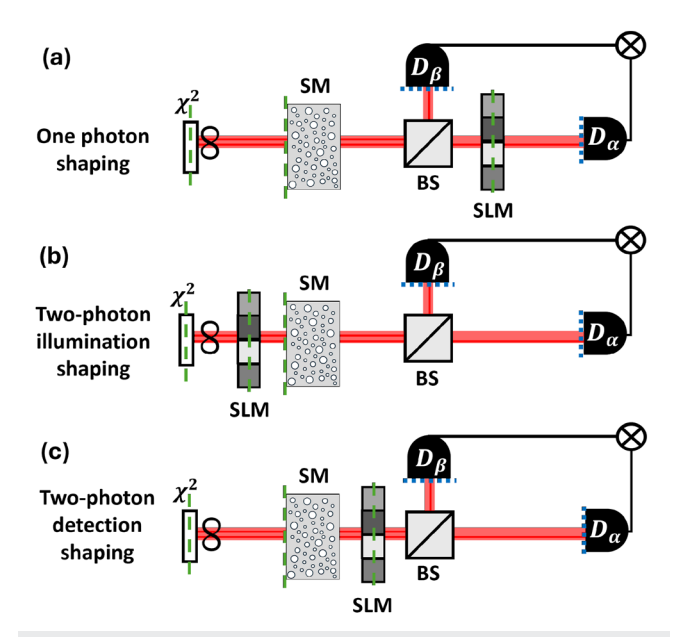


**FIG. 1.** The three configurations for wavefront shaping of spatially entangled photons analyzed in this work. In all configurations, entangled photons are generated in a  $\chi^{(2)}$  SPDC process (type-I), and then propagate through a scattering medium (SM). Their correlations are detected using coincidence events between two single-photon detectors ( $D_{\alpha}$ ,  $D_{\beta}$ ). (a) The onephoton shaping configuration, where only one of the photons is shaped. (b) The two-photon illumination shaping configuration, where the SLM shapes both photons before propagating through the scattering medium. (c) The two-photon detection shaping configuration, where the SLM is positioned after the scattering sample and shapes both photons. The green dashed lines mark conjugate planes, and the dotted blue lines mark the far field of these planes.

a lossless multimode fiber with strong mode mixing. (ii) A matrix whose elements are independently and identically distributed random variables drawn from a circular complex Gaussian distribution (Gaussian IID),<sup>39</sup> representing a subspace of a strongly scattering medium.<sup>40</sup>

As depicted in Fig. 1, we analyze three different configurations for positioning an SLM to compensate for this scattering. In the first configuration [Fig. 1(a)], the SLM is placed after the scattering medium and shapes only one of the photons. We refer to this configuration as one photon shaping (1P-S). In the second configuration [Fig. 1(b)], the SLM is placed before the scattering medium and shapes both photons. We call this configuration two-photon illumination shaping (2P-IS). In the third configuration [Fig. 1(c)], the SLM is placed after the scattering medium and shapes both photons. We refer to it as two-photon detection shaping (2P-DS). In all three configurations, we assume the SLM is placed in the image plane of the input facet of the scattering medium and of the nonlinear crystal, such that the two photons illuminate the same area on the sample, and the detectors are placed at its far-field.

The goal of the wavefront shaping schemes we consider is to maximize the probability to find the photons in two spatial modes  $\alpha$  and  $\beta$ , corresponding to a coincidence event. For the three configurations we consider, this probability is given by (see supplementary material Sec. S1):

$$\begin{split} P_{\alpha\beta}^{(1P-S)} &= \frac{1}{2N} \left| \left( \mathcal{F}TT^{\mathsf{T}} S \mathcal{F} \right)_{\beta\alpha} \right|^{2}, \\ P_{\alpha\beta}^{(2P-IS)} &= \frac{1}{2N} \left| \left( \mathcal{F}TSST^{\mathsf{T}} \mathcal{F} \right)_{\beta\alpha} \right|^{2}, \\ P_{\alpha\beta}^{(2P-DS)} &= \frac{1}{2N} \left| \left( \mathcal{F}STT^{\mathsf{T}} S \mathcal{F} \right)_{\beta\alpha} \right|^{2}, \end{split} \tag{1}$$

where S is a diagonal matrix representing the operation performed by the SLM in the pixel basis, and  $\mathcal{F}$  is the discrete Fourier transform operator, representing the propagation to the detectors plane in the far-field.

To gain further physical intuition into these three configurations, it is useful to interpret them using Klyshko's advanced wave picture.  $^{31,41-43}$  In this picture, the probability P for a coincidence event between two single-photon detectors in a two-photon setup is translated to a classical intensity measurement by substituting one of the detectors with a classical light source and the nonlinear crystal with a mirror. The light emitted from this source is directed back through the optical setup toward the mirror and is then reflected to the second detector. According to the advanced wave picture, the intensity measured at the second detector is proportional to the average coincidence rate observed in the original two-photon experiment. In Fig. 2, we show the advanced wave interpretation of the three configurations described in Fig. 1. While the calculations yield the same expressions in both pictures (see supplementary material Sec. S1), the advanced wave picture provides several physical insights that help interpret the three configurations.

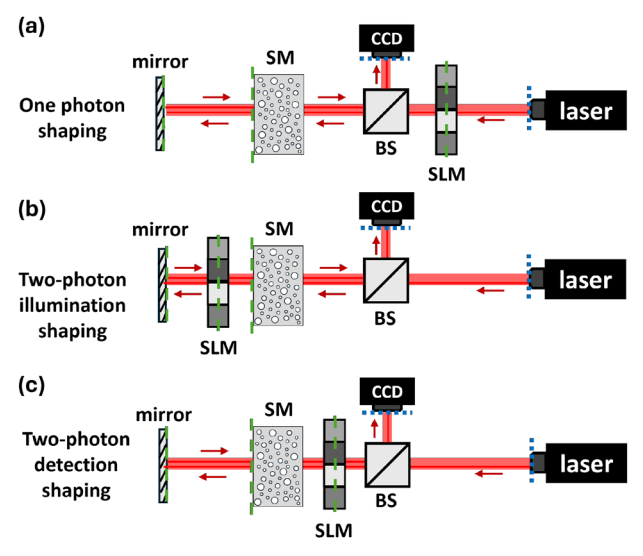


FIG. 2. Depiction of the three analogous classical setups according to the advanced wave picture. (a) The analogous 1P-S configuration, which is a classical wavefront shaping scenario in reflection geometry. (b) The analogous 2P-IS configuration, where the light is scattered both before and after being shaped by the SLM. (c) The analogous 2P-DS configuration, involving light impinging on the same SLM twice: before and after the scattering medium. The green dashed lines mark conjugate planes, and the dotted blue lines mark their far-field plane.

### A. One photon shaping (1P-S)

We begin by analyzing the 1P-S configuration, where only one of the SPDC photons is shaped. As shown by the advanced wave interpretation [Fig. 2(a)], this case is equivalent to a standard classical wavefront-shaping experiment in a reflection geometry, where light traverses the medium twice. The problem thus reduces to maximizing the intensity of a classical coherent field emitted from mode  $\alpha$  and detected at mode  $\beta$ .

The figure of merit we use to define the optimization quality is the enhancement factor  $\eta$ . This is defined as the ratio between the maximal coincidence probability  $P_{\alpha\beta}$ , achieved by optimizing the SLM phases, and the spatially averaged coincidence probability before optimization. As we show explicitly in the supplementary material Sec. S2, for 1P-S and a phase-only SLM, the enhancement is given by

$$\eta_{1P-S} = 1 + (N-1)\frac{\pi}{4},$$
(2)

where N denotes the number of modes in the system. This reproduces the well-known classical result of linear scaling in N with a pre-factor of  $\frac{\pi}{4}$  for phase-only control.<sup>35</sup>

While the enhancement is the same for the unitary and Gaussian IID cases, the peak-to-background ratio is different. In the  $N\gg 1$  limit, the peak in both cases is  $\eta/N\approx \pi/4$ . However, in the unitary case, the background is  $1-\eta/N$ , since the peak gets its power from the background, while for Gaussian IID, the total background power is higher.

### B. Two-photon illumination shaping (2P-IS)

We now consider the 2P-IS configuration [Fig. 1(b)], where the SLM shapes both photons before the scattering medium. The SLM is typically placed in an image plane of the crystal to ensure the phase mask *S* acts identically on both photons, as described in Eq. (1) by SS. In the advanced wave counterpart [Fig. 2(b)], this corresponds to a configuration in which the light is scattered both before and after passing through the SLM. Here, the fact that the SLM is in the image plane of the crystal implies that the light hits the SLM twice with the same spatial distribution, effectively equivalent to a single pass where each pixel induces a double phase.

By performing an analytical calculation similar to that of the 1P-S configuration (see supplementary material Sec. S2), we obtain

$$\eta_{2P-IS} = 1 + (N-1) \left(\frac{\pi}{4}\right)^2.$$
(3)

For  $N\gg 1$ , the enhancement is lowered by a factor of  $\pi/4$  compared to  $\eta_{1P-S}$ . This can be intuitively understood in the advanced wave picture: in this configuration, the SLM is illuminated with a speckle pattern with varying amplitude, so that some of its N pixels contribute less effectively to the optimization, leading to a reduced number of effective degrees of control.

# 1. Enhanced correlations by digital optical phase conjugation

Although the 2P-IS configuration typically results in a lower enhancement, a remarkable effect occurs when optimizing the probability  $P_{\alpha\alpha}$  that both photons are detected in the *same* spatial mode, namely, when the transverse positions of the two detectors

are identical. In this symmetric case, the two-photon correlation enhancement is given by

$$\eta_{2P-IS}^{(OPC)} = N + b, \tag{4}$$

where b=0 for the unitary case and b=1 for the Gaussian IID case. Remarkably, the enhancement scales linearly with the number of modes with a pre-factor of exactly 1, despite the use of phase-only modulation. Before optimization, upon detection of a photon in some mode  $\alpha$ , the probability to detect its twin photon in some specific mode is, on average, 1/N. After optimization, the probability to detect the twin photon in mode  $\alpha$  becomes unity. Notably, in the unitary case, there is no residual background  $(1-\eta/N=0)$ , manifesting the *perfect* enhancement achieved. Further details are given in the supplementary material Sec. S2.

It is instructive to interpret the perfect correlations obtained when the two photons are detected in the same mode as digital optical phase conjugation in the advanced wave picture. <sup>44</sup> Perfect correlations, which correspond in the advanced wave picture to focusing all the light back toward the source, are obtained when the phases applied by the SLM are the conjugate of the field incident on it after passing through the scattering sample [Fig. 2(b)]. In this case, the field after the SLM becomes the phase conjugate of the incident field. By time-reversal symmetry, this results in all the light being focused back toward the sources. <sup>45</sup>

In contrast to typical digital optical phase conjugation configurations, where perfect time reversal requires precise control over both the amplitude and phase of the scattered field, here perfect time reversal is achieved using phase conjugation alone. This is possible because, in the advanced wave picture, the SLM is placed after the scattering medium. As a result, the amplitude of the field illuminating the SLM is already correct, and only the phases need to be conjugated. We emphasize that the SLM appears after the scattering medium only in the advanced wave picture. In practice, the SLM shapes the two photons before they illuminate the sample. We refer to this special configuration as 2P-IS(OPC).

## C. Two-photon detection shaping (2P-DS)

Next, we consider the 2P-DS configuration, where the SLM shapes the two photons *after* the scattering medium [Fig. 1(c)]. In the advanced wave picture [Fig. 2(c)], the light now encounters the same SLM twice, with random scattering occurring in between the two encounters.

The advanced wave picture highlights that the 2P-DS poses a significant optimization challenge: attempting to optimize the SLM phases using standard iterative algorithms<sup>4</sup> fails because the SLM pixels are no longer independent. The phase applied to one pixel affects not only the light that is reflected from that pixel but also the light that will impinge on other pixels when the beam illuminates the SLM for the second time. In the supplementary material Sec. S3, we show that maximizing the two-photon correlations in the 2P-DS case can be mapped to a version of a maximum quadratic program (MAXQP) or to finding the ground state of an XY Ising model, which are known to be NP-hard problems. <sup>32,46-51</sup>

Despite this computational complexity, we use PyTorch's autograd engine for gradient-based optimization of phase patterns that localize the correlations between two target modes, in a system

with N=512 modes. Full details are provided in the supplementary material Sec. S4 and in the supplementary code. <sup>52</sup> Unlike the 1P-S and 2P-IS configurations, in this scenario our simulations reveal distinct behavior for unitary and Gaussian IID transmission matrices: for the unitary case, we find a value of  $\eta_{2p-DS}^{(U)}\approx 0.89\cdot N$ , and for the Gaussian IID case, our optimization yields a remarkable enhancement of  $\eta_{2p-DS}^{(G)}\approx 1.91\cdot N$ , such that the coincidence rate between the optimized modes exceeds the total coincidence rate before optimization. This is possible since the shaping process could redirect photons that would otherwise be scattered into unmeasured modes, such as reflected channels in the case of a scattering medium, into the measured ones. In both cases, the enhancement pre-factor slightly increases with the system size N, as we discuss in the supplementary material Sec. S4.

Self-consistent optimization is not a unique feature of the 2P-DS configuration and may also arise in the 2P-IS configuration, for instance, when the SLM is not imaged onto the nonlinear crystal, as we discuss in the supplementary material Sec. S5.

# 1. Enhanced correlations by digital optical phase conjugation

Similarly to the 2P-IS configuration, also in detection shaping we observe that maximizing the probability that both photons arrive at the same detector increases the enhancement factor. For the unitary case, we once again numerically achieve a perfect enhancement of  $\eta_{2P-DS}^{(OPC)} = N$ . We interpret this as a more intricate version of digital optical phase conjugation in the advanced wave picture [Fig. 2(c)]. In this picture, for the reflected field to be the time-reversed version of the incident field, the reflection process at the mirror must correspond to phase conjugation. First, we note that if the phases arrive at the mirror plane with a flat phase, it will effectively act as a phase-conjugating mirror, since the phase conjugation of a flat phase is a flat phase. Similarly, if the field in the mirror plane is real-valued, namely the phases are only 0 or  $\pi$ , the mirror effectively acts as a phase-conjugating mirror. Thus, the optimal phases that the SLM finds in this configuration are such that the field at the mirror plane is real (see Fig. S5). Since there are two possible phases for each mode, there are  $2^N$  such solutions, and it is thus relatively simple for the optimization process to find such a solution and achieve perfect correlations. We refer to this special configuration as 2P-DS(OPC).

For Gaussian IID transmission matrices, the enhancement is not bounded from above by N, and we find numerically an enhancement of  $\eta_{2P-DS}^{(OPC)} \approx 4.6 \cdot N$ . While we do not have a physical explanation for the enhancement value in the Gaussian IID case, we note that it is bounded by  $\sigma_1^2$ , where  $\sigma_1$  is the maximal singular value of  $TT^T$ . Physically,  $\sigma_1^2$  corresponds to the maximal intensity transmission through the medium.

We summarize the enhancement pre-factors of the different configurations in Fig. 3. Notably, it highlights that the 2P-DS configuration puts forward a unique problem, where on one hand the optimization is hard and self-consistent, but on the other hand holds the potential for greatly improved performance, particularly in the symmetric configuration. To complement these results, in the supplementary material Sec. S6, we also analyze the case of a thin diffuser.

**ARTICLE** 

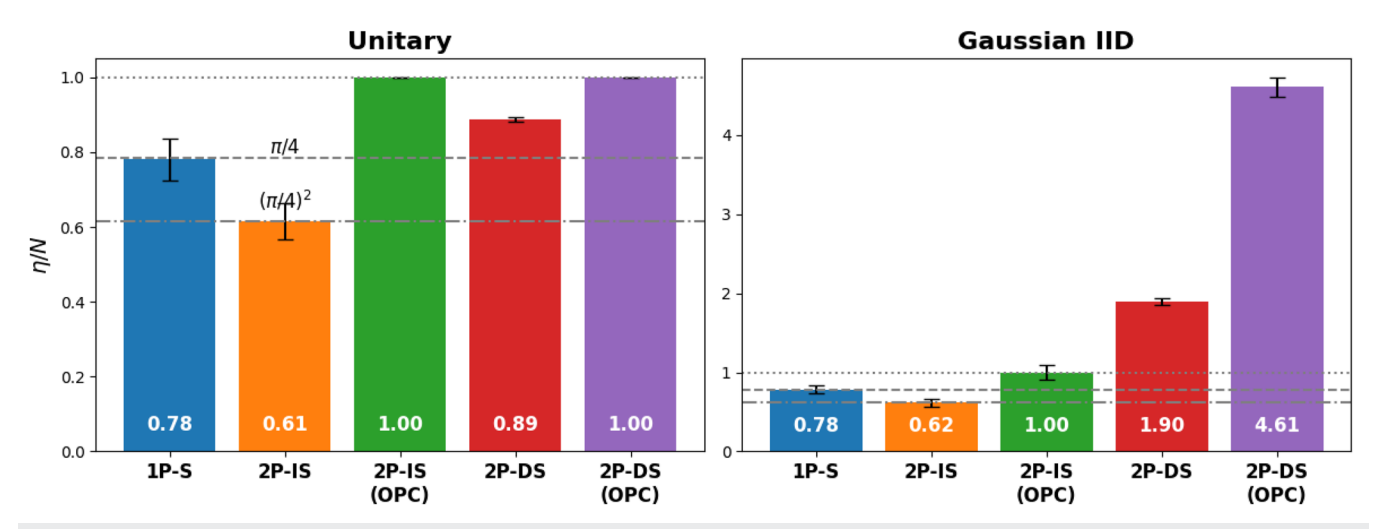


**FIG. 3.** Summary of the enhancement pre-factor for the five different analyzed configurations. The enhancements were calculated numerically by averaging over 200 disorder realizations, for a system with 512 modes. The error bars signify the standard deviation of the 200 realizations. The 1P-S, 2P-IS, and 2P-IS(OPC) configurations present the same results for the unitary and Gaussian IID cases, and agree with the analytical calculations of  $\pi/4$ ,  $(\pi/4)^2$ , and 1, respectively. The 2P-DS and 2P-DS(OPC) configurations are significantly different for the unitary and Gaussian IID cases. In the latter, the coincidence rate between the optimized modes exceeds the total coincidence rate prior to optimization.

# D. Incomplete control

In most practical applications, the number of modes controllable via the SLM is limited and is often less than the total number of modes supported by the scattering medium. We denote this as incomplete control and simulate how it influences the achievable enhancement  $\eta$  in the different configurations. We define the degree of control (DOC) as the ratio between the number of controlled modes M (e.g., independent SLM pixels) and the total number of modes considered in the system N. Figure 4 illustrates the scaling of the enhancement pre-factor  $\eta/N$  as a function of the degree of control for unitary and Gaussian IID transmission matrices.

First, we analyze the unitary case. For the 1P-S configuration, the enhancement exhibits a linear dependence on the DOC, consistent with classical wavefront shaping results, where enhancement scales linearly with the number of controlled modes (see supplementary material Sec. S6).

The 2P-IS configuration displays nonlinear scaling. As shown analytically in the supplementary material Sec. S6, the initial slope at low DOC is  $\pi/4$ . Since the enhancement pre-factor reaches  $(\pi/4)^2$  at full control (DOC = 1), the curve shows a decreasing slope, indicating a diminishing gain in enhancement as the degree of control increases. Intuitively, at a low degree of control, the SLM has large effective macro-pixels that average out the speckle illumination, effectively restoring a uniform beam condition akin to the 1P-S configuration.

The symmetric 2P-IS(OPC) configuration also shows non-linear scaling with a decreasing slope. As derived in the supplementary material, the initial slope at a low degree of control is  $\pi/2 \approx 1.57$ , while the enhancement pre-factor reaches 1 at full control. This initial slope is notably twice the  $\pi/4$  slope observed at low degrees of control for the non-symmetric 2P-IS case. This factor-of-two difference in the initial enhancement rate is reminiscent of

coherent backscattering (CBS).<sup>38,53</sup> Standard CBS describes the enhanced average intensity back-reflected into the incident mode from a disordered medium, arising without any wavefront shaping, due to constructive interference between pairs of reciprocal paths inside the sample. Here, this constructive interference results in a two-fold improvement of the enhancement factor at low degrees of control, since in the advanced wave picture, the 2P-IS(OPC) configuration corresponds to a CBS setting.<sup>54</sup>

Considering the unitary case, the 2P-DS configurations also exhibit nonlinear scaling with a decreasing slope. For the symmetric OPC case, this particularly efficient approach to high enhancement can be intuitively understood by recalling that there are  $2^N$  valid options for phases in the mirror plane that will all result in a perfect enhancement. Thus, even when the control is incomplete, the existence of this vast solution space allows a fraction of these solutions to remain approximately reachable, leading to the observed saturation behavior at near-maximal enhancement even for DOC significantly less than 1 (see Fig. S8).

Next, we consider the Gaussian IID case. The 1P-S, 2P-IS, and 2P-IS(OPC) configurations exhibit scaling behaviors very similar to their unitary counterparts: linear for 1P-S, and nonlinear with a decreasing slope for both 2P-IS cases. However, the 2P-DS configurations behave distinctly in the Gaussian IID case, showing nonlinear scaling with an increasing slope.

Even though we do not have an analytic model for the 2P-DS configuration, we empirically perform a linear fit to the slope of these configurations in the regime of low degree of control (see Fig. S7). We observe that in both the unitary and Gaussian IID cases, the initial slope of the symmetric 2P-DS(OPC) configuration is approximately twice that of the non-symmetric counterpart. This consistent factor-of-two difference reinforces the analogy to an extended CBS-like effect influencing the initial optimization efficiency.

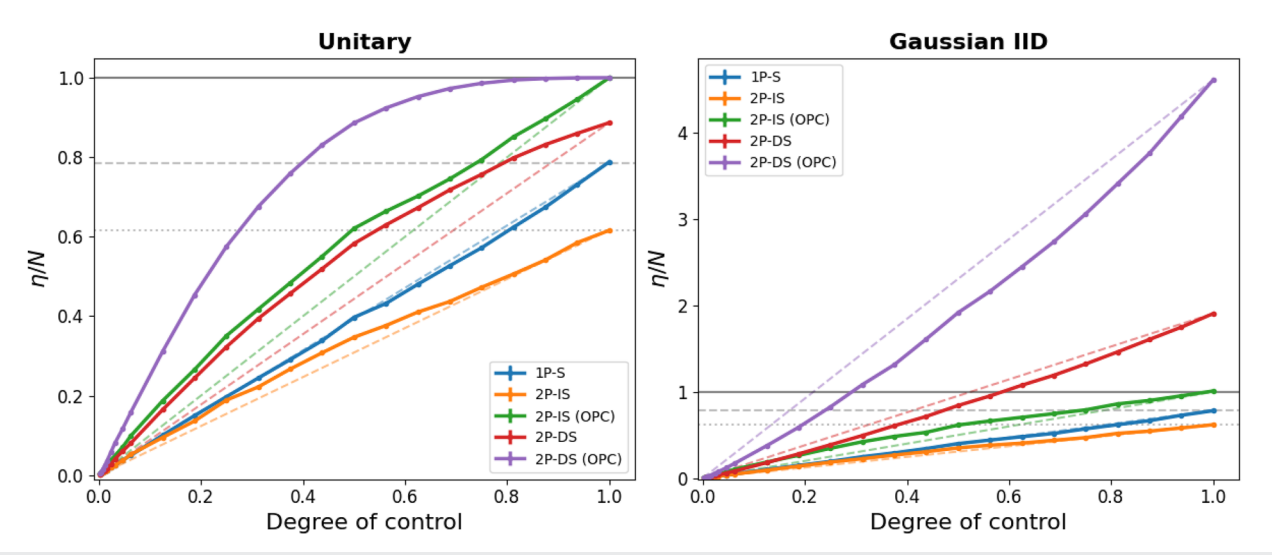


**FIG. 4.** Scaling of the enhancement pre-factor as a function of the degree of control, defined as the ratio DOC = M/N between the number of SLM pixels M and the number of modes in the system N, for the analyzed configurations with unitary and Gaussian IID matrices. Dashed straight lines connect the endpoints for each curve to guide the eye regarding linear or nonlinear scaling. The results are shown for N = 512.

# E. Non-maximally entangled state

The calculations and numerical simulations presented thus far assumed that the generated SPDC photons are in a maximally entangled state,  $|\Psi_{\rm in}\rangle = \frac{1}{\sqrt{2N}}\sum_n\hat{a}_n^{\dagger}\hat{a}_n^{\dagger}|{\rm vac}\rangle$ . However, in practice, the state generated by the SPDC is given by  $^{36,55}$   $|\Psi\rangle \propto \iint d{\bf q}_{\rm s}d{\bf q}_{\rm i}\nu$   $({\bf q}_{\rm s}+{\bf q}_{\rm i}){\rm sinc}(\frac{L_c}{4k_p}|{\bf q}_{\rm s}-{\bf q}_{\rm i}|^2)|{\bf q}_{\rm s},{\bf q}_{\rm i}\rangle$ , where  $\nu({\bf q})$  is the angular spectrum of the pump beam,  $L_c$  is the crystal length,  $k_p$  is the wavenumber of the pump beam, and  ${\bf q}_{\rm s}$  and  ${\bf q}_{\rm i}$  represent the transverse momentum of the signal and idler photons. Using the Schmidt decomposition,  $^{56,57}$  the two-photon state may be written as a sum of K states, each composed of a tensor product between one-photon states. The Schmidt rank K quantifies the entanglement dimensionality.

Our analysis thus far assumed a plane-wave pump beam, such that  $v(\mathbf{q}) \approx \delta(\mathbf{q})$  and a thin crystal such that  $\mathrm{sinc}(\frac{L_c}{4k_p}|\mathbf{q_s}-\mathbf{q_i}|^2)$   $\approx$  const. This results in a maximally entangled state with an infinite Schmidt rank. When this state illuminates a sample with a finite size, supporting N modes, we assume that it is truncated to the subspace spanned by the modes of the sample and can therefore be described by a maximally entangled state with Schmidt rank N.

To incorporate the effect of a finite pump profile and finite crystal length, we invoke the advanced wave picture. <sup>31,43</sup> To account for the finite pump beam size, the crystal acts as a mirror whose reflectivity at each position is proportional to the local pump amplitude. The finite crystal length in the advanced wave picture is accounted for by introducing a spatial filter that removes the angular components that are not phase-matched in the SPDC process. <sup>31,43</sup> Both of these effects can be regarded as applying the appropriate spatial filters to the two-photon state in the position (near-field) and momentum (far-field) domains. In the supplementary material Sec. S1, we show that this description can be generalized so that any pure two-photon state can be mapped to a maximally entangled state passing through a fictitious linear system.

To analyze the case of non-maximally entangled states, we need to consider the three configurations 1P-S [Fig. 2(a)], 2P-IS [Fig. 2(b)], and 2P-DS [Fig. 2(c)], with the appropriate spatial filters. In the 1P-S and 2P-DS configurations, these filters are sandwiched between two passages through the scattering sample. We can, therefore, attribute the filters to a new, fictitious, filtered sample. The problem then reduces to the propagation of a maximally entangled state with Schmidt rank K = N through the fictitious sample, allowing us to apply the results obtained above for maximally entangled states, with the caveat that the sample properties (e.g., being unitary or Gaussian IID) may be modified by the filters.

In contrast, in the 2P-IS shaping configuration, we cannot use the fictitious sample model because the SLM is also sandwiched between the two interactions with the sample. Here, the spatial filters qualitatively change the optimization: the finite pump profile will result in a non-uniform illumination on the SLM, which is known from classical wavefront shaping to slightly affect the enhancement.<sup>58</sup> Furthermore, the spatial filtering will cause the light shaped by an SLM pixel on the first pass to affect the light hitting its neighboring pixels on the second pass, resulting in a self-consistent optimization problem. This effect can also be understood in the direct SPDC picture, without invoking the advanced wave picture: the spatial filter accounts for the finite correlation width of the two photons upon illumination of the SLM. A correlation width that is comparable to the SLM pixel size leads to a non-convex optimization landscape, as demonstrated in Ref. 32. Notably, the width of the spatial envelope and the angular width of the spatial filter can be traded off by magnifying or de-magnifying the SPDC light between the crystal and SLM planes.

#### 1. Separable state

An extreme limit of the spatial filtering is when the widths of the pump angular spectrum and of the sinc function are equal, resulting in a separable state, and a Schmidt rank K = 1.56 In this limit, it

is convenient to analyze the system in the direct SPDC picture and not in the advanced wave picture. Since the two photons are now in a separable state, a speckle pattern will also be observed in the single counts (i.e., intensity) at the detectors' plane, and the coincidence measurements are equivalent to multiplying the intensities at the two detector locations. <sup>16,59</sup> In the 1P-S configuration, maximizing the two-photon correlations is equivalent to performing classical wavefront shaping. Enhancing the intensity at only one of the detectors yields the classical enhancement of  $\eta \approx (\pi/4)N$ . This is also the total enhancement of the correlations, since the speckle pattern at the second detector is unaffected. In the advanced wave picture, this is equivalent to shaping light that is propagating through a scattering medium with a single-mode pinhole in the middle—a system that has been of interest in Ref. 60, due to the long-range correlations that emerge in such a system.

In the 2P-DS configuration, the SLM affects the two speckle patterns that arrive at the two planes of the detectors identically. Therefore, if both detectors are at the same location (OPC configuration), focusing to one detector will also focus the light to the second detector, resulting in an enhancement of  $\eta_{K=1}^{(OPC)} = (\pi/4 \cdot N)^2$  to the correlations. If the two detectors are located at different transverse positions, one-half of the SLM pixels could be used to focus at one position and the other half to focus at the second position, resulting in a total enhancement of  $\eta_{K=1} = (\pi/4 \cdot N/2)^2$  to the correlations. In the 2P-IS configuration, assuming that the low Schmidt rank

In the 2P-IS configuration, assuming that the low Schmidt rank originates from a tightly focused pump, and given that the crystal is imaged onto the SLM, only a single SLM pixel will have an effect, resulting in no enhancement. If, however, the SLM is placed in the far field of the crystal, such that all SLM pixels are active, the results

are identical to the 2P-DS configuration. Since for K=1, the signal we are focusing is the single counts, and this is like classical wavefront shaping where it does not matter whether the SLM is placed before or after the scattering medium. We refer to this configuration with the SLM at the far field of the crystal as 2P-IS-ff.

# 2. Numerical simulation

While an exact analysis for the dependence on the two-photon state requires a full field simulation that takes into account the finite pump width and crystal dimensions, we roughly simulate a finite Schmidt rank K by blocking N-K modes at the crystal plane and optimizing coincidence events. This corresponds in the experiment to a top-hat pump beam of varying width and a thin crystal. The results are depicted in Fig. 5 for N=512 for both the unitary and Gaussian IID models. At low Schmidt ranks, the 2P-IS-ff and 2P-DS configurations result in equal enhancement factors, with the expected  $\eta_{K=1}^{(OPC)}$  and  $\eta_{K=1}$  values for K=1, which are quadratic in N.

This changes as K grows, and for K=N, the 2P-DS returns to the enhancements discussed in Sec. II, which are approximately linear in N (see supplementary material Sec. S4). The 2P-IS-ff configuration reaches reduced enhancements at K=N, since when the SLM is placed in the far field of the crystal, pixel pairs that are symmetrically placed across the optical axis are degenerate, resulting in a lower amount of effective SLM pixels. Indeed, the results for K=N in the 2P-IS-ff configurations are identical to the results for the 2P-IS configurations with a degree of control of 0.5. The 1P-S configuration allows an enhancement of  $\approx \pi/4 \cdot N$  independent of K. The full simulation code is available in Ref. 52.

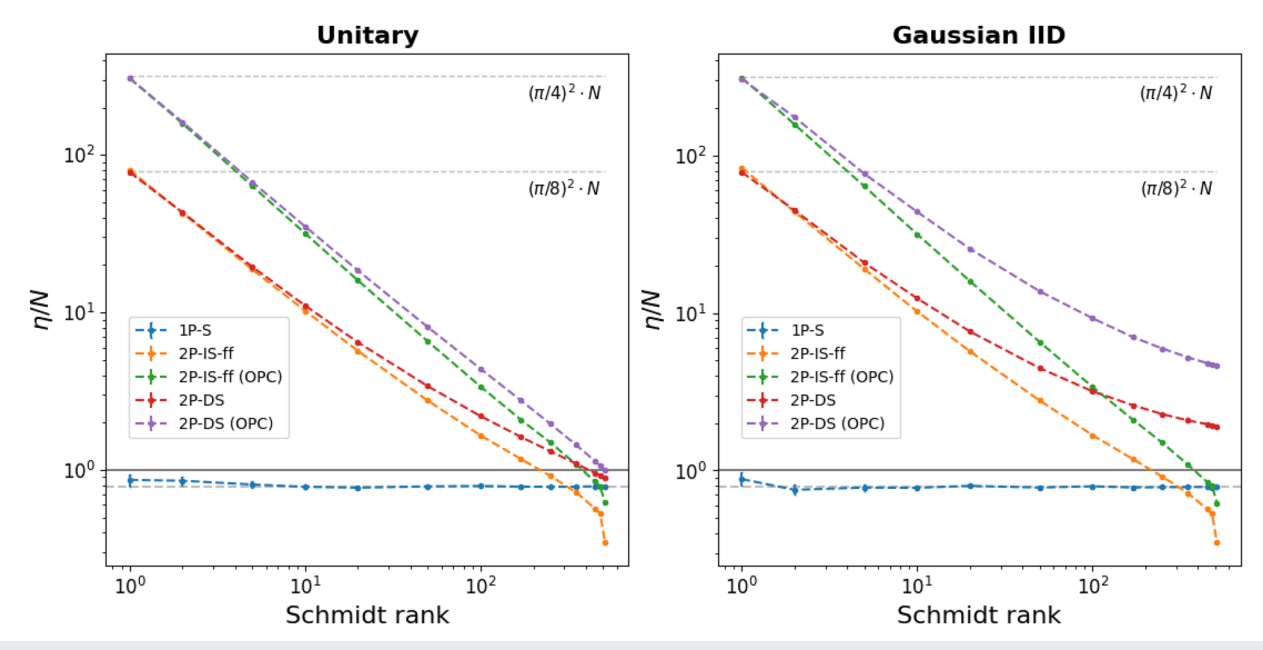


**FIG. 5.** The ratio of the enhancement to the number of modes  $\eta/N$  as a function of the Schmidt rank K of the two-photon state. The 2P-IS-ff configuration is similar to the 2P-IS configuration (SLM between the crystal and the scattering medium), but with the SLM in the far field of the crystal. For low K, focusing the coincidence rate also focuses the single counts, yielding an enhancement that scales quadratically with N. For high K, the single counts are uniform, and the enhancement scales linearly with N. The results are shown for both the unitary and Gaussian IID cases with N = 512, on a log-log scale.

#### III. DISCUSSION

In this work, we have shown that, unlike in classical wavefront shaping, the specific placement and configuration of the SLM and detectors play a crucial role in determining the achievable enhancement when shaping entangled photons that both propagate through a thick scattering medium. Beyond their intrinsic interest, configurations where both photons traverse the medium also serve as a platform for applications that use complex media to implement tailored quantum circuits<sup>24,61-63</sup> and to study fundamental aspects of quantum light in complex media. <sup>54,64-67</sup>

We found that two-photon wavefront shaping gives rise to a rich variety of behaviors with no direct counterpart in the classical regime. Depending on the configuration, two-photon correlations can either enhance or reduce performance compared to classical shaping and can exhibit fundamentally new features. For example, in the 2P-IS configuration, a natural symmetry of the two-photon measurement enables perfect compensation of scattering when focusing both photons to the same spatial mode, despite relying on phase-only control.

In the 2P-DS configuration, where photons impinge twice on the SLM, leading to correlated pixel control, we have found a significant boost in enhancement. This improvement, however, comes at the price of a fundamentally more challenging, self-consistent optimization problems. Similar self-consistent optimization problems arise in advanced classical systems, such as coherent confocal microscopy through scattering media<sup>68</sup> and tunable metasurface reflect-arrays inside chaotic microwave cavities.<sup>69</sup> Interestingly, while presenting a challenge for optimization, the interdependence of pixels has been leveraged in optical information processing and neural networks, enabling nonlinear operations using linear optics.<sup>70,71</sup>

The emergence of complex feedback mechanisms in two-photon coincidence measurements highlights new opportunities to exploit quantum correlations. Observing these effects experimentally will be subject to the standard challenges of wavefront shaping at low light levels, such as low collection efficiencies and limited signal-to-noise ratios. Nevertheless, wavefront shaping of single and entangled photons has been shown to be feasible over the past decade. <sup>18,20,22,31,32</sup> Our analysis of the robustness of the observed performance under incomplete control and non-ideal quantum states points to two additional challenges that are more unique to the observation of the fundamental bounds discussed in this work, while at the same time emphasizing the experimental feasibility of demonstrating them.

We believe that these findings provide important insights into the foundations of quantum wavefront shaping and offer practical considerations for shaping entangled photons through complex media, with potential applications ranging from quantum imaging to secure communications.

## SUPPLEMENTARY MATERIAL

See the <u>supplementary material</u> for analytical derivations, exploration of other configurations, and further details regarding the numerical simulations, which may be found in the attached document.

#### **ACKNOWLEDGMENTS**

The authors would like to thank Ohad Lib, Anat Levin, and Ori Katz for many fruitful discussions.

This research was supported by the Zuckerman STEM Leadership Program and the Israel Science Foundation (Grant No. 2497/21). R.S. acknowledges the support of the Israeli Council for Higher Education and of the HUJI Center for Nanoscience and Nanotechnology. S.M.P acknowledges the French *Agence Nationale pour la Recherche* Grant No. ANR-23-CE42-0010-01 and the Labex WIFI Grant Nos. ANR-10-LABX-24 and ANR-10-IDEX-0001-02 PSL\*.

#### **AUTHOR DECLARATIONS**

#### **Conflict of Interest**

The authors have no conflicts to disclose.

#### **Author Contributions**

Ronen Shekel: Conceptualization (lead); Formal analysis (lead); Investigation (lead); Software (lead); Writing – original draft (lead); Writing – review & editing (lead). Sébastien M. Popoff: Formal analysis (supporting); Investigation (supporting); Writing – review & editing (equal). Yaron Bromberg: Conceptualization (equal); Formal analysis (equal); Funding acquisition (lead); Methodology (equal); Supervision (lead); Writing – original draft (equal); Writing – review & editing (equal).

#### **DATA AVAILABILITY**

The data that support the findings of this study are openly available in Zenodo at https://doi.org/10.5281/zenodo.17036996.<sup>52</sup>

### **REFERENCES**

- <sup>1</sup>I. M. Vellekoop and A. P. Mosk, "Focusing coherent light through opaque strongly scattering media," Opt. Lett. **32**, 2309–2311 (2007).
- <sup>2</sup>A. P. Mosk, A. Lagendijk, G. Lerosey, and M. Fink, "Controlling waves in space and time for imaging and focusing in complex media," Nat. Photonics **6**, 283–292 (2012)
- <sup>3</sup>S. M. Popoff, G. Lerosey, R. Carminati, M. Fink, A. C. Boccara, and S. Gigan, "Measuring the transmission matrix in optics: An approach to the study and control of light propagation in disordered media," Phys. Rev. Lett. **104**, 100601 (2010).
- <sup>4</sup>I. M. Vellekoop, "Feedback-based wavefront shaping," Opt. Express 23, 12189–12206 (2015).
- <sup>5</sup>H. Cao, A. P. Mosk, and S. Rotter, "Shaping the propagation of light in complex media," Nat. Phys. **18**, 994–1007 (2022).
- <sup>6</sup>S. Gigan, O. Katz, H. B. De Aguiar, E. R. Andresen, A. Aubry, J. Bertolotti, E. Bossy, D. Bouchet, J. Brake, S. Brasselet *et al.*, "Roadmap on wavefront shaping and deep imaging in complex media," J. Phys.: Photonics 4, 042501 (2022).
- <sup>7</sup>O. Lib and Y. Bromberg, "Quantum light in complex media and its applications," Nat. Phys. **18**, 986–993 (2022).
- <sup>8</sup>S. K. Goyal, A. H. Ibrahim, F. S. Roux, T. Konrad, and A. Forbes, "The effect of turbulence on entanglement-based free-space quantum key distribution with photonic orbital angular momentum," J. Opt. 18, 064002 (2016).
- <sup>9</sup>B. Ndagano, B. Perez-Garcia, F. S. Roux, M. McLaren, C. Rosales-Guzman, Y. Zhang, O. Mouane, R. I. Hernandez-Aranda, T. Konrad, and A. Forbes, "Characterizing quantum channels with non-separable states of classical light," Nat. Phys. 13, 397–402 (2017).

- <sup>10</sup>C. Liu, K. Pang, Z. Zhao, P. Liao, R. Zhang, H. Song, Y. Cao, J. Du, L. Li, H. Song *et al.*, "Single-end adaptive optics compensation for emulated turbulence in a Bi-directional 10-Mbit/s per channel free-space quantum communication link using orbital-angular-momentum encoding," Research 2019, 8326701.
- <sup>11</sup> Y. Cao, Y.-H. Li, K.-X. Yang, Y.-F. Jiang, S.-L. Li, X.-L. Hu, M. Abulizi, C.-L. Li, W. Zhang, Q.-C. Sun *et al.*, "Long-distance free-space measurement-device-independent quantum key distribution," Phys. Rev. Lett. **125**, 260503 (2020).
- <sup>12</sup> L. V. Amitonova, T. B. H. Tentrup, I. M. Vellekoop, and P. W. H. Pinkse, "Quantum key establishment via a multimode fiber," Opt. Express 28, 5965–5981 (2020).
- <sup>13</sup>C. J. Pugh, J.-F. Lavigne, J.-P. Bourgoin, B. L. Higgins, and T. Jennewein, "Adaptive optics benefit for quantum key distribution uplink from ground to a satellite," Adv. Opt. Technol. **9**, 263–273 (2020).
- <sup>14</sup>R. Abolhassani, L. Scarfe, F. Di Colandrea, A. D'Errico, K. Heshami, and E. Karimi, "Investigating the performance of adaptive optics on different bases of spatial modes in turbulent channels," arXiv:2508.21015 (2025).
- <sup>15</sup>C. W. J. Beenakker, J. W. F. Venderbos, and M. P. van Exter, "Two-photon speckle as a probe of multi-dimensional entanglement," Phys. Rev. Lett. 102, 193601 (2009).
- <sup>16</sup>W. H. Peeters, J. J. D. Moerman, and M. P. van Exter, "Observation of two-photon speckle patterns," Phys. Rev. Lett. **104**, 173601 (2010).
  <sup>17</sup>J. Carpenter, C. Xiong, M. J. Collins, J. Li, T. F. Krauss, B. J. Eggleton, A. S.
- <sup>17</sup>J. Carpenter, C. Xiong, M. J. Collins, J. Li, T. F. Krauss, B. J. Eggleton, A. S. Clark, and J. Schröder, "Mode multiplexed single-photon and classical channels in a few-mode fiber," Opt. Express 21, 28794–28800 (2013).
- <sup>18</sup>H. Defienne, M. Barbieri, B. Chalopin, B. Chatel, I. A. Walmsley, B. J. Smith, and S. Gigan, "Nonclassical light manipulation in a multiple-scattering medium," Opt. Lett. 39, 6090–6093 (2014).
- <sup>19</sup>T. J. Huisman, S. R. Huisman, A. P. Mosk, and P. W. H. Pinkse, "Controlling single-photon Fock-state propagation through opaque scattering media," Appl. Phys. B 116, 603–607 (2014).
- <sup>20</sup>N. H. Valencia, S. Goel, W. McCutcheon, H. Defienne, and M. Malik, "Unscrambling entanglement through a complex medium," Nat. Phys. 16, 1112–1116 (2020).
- <sup>21</sup> R. Shekel, O. Lib, R. Gutiérrez-Cuevas, S. M. Popoff, A. Ling, and Y. Bromberg, "Shaping single photons through multimode optical fibers using mechanical perturbations," APL Photonics 8, 096109 (2023).
- <sup>22</sup>F. Devaux, A. Mosset, S. M. Popoff, and E. Lantz, "Restoring and tailoring very high dimensional spatial entanglement of a biphoton state transmitted through a scattering medium," J. Opt. 25, 055201 (2023).
- H. Defienne, M. Barbieri, I. A. Walmsley, B. J. Smith, and S. Gigan, "Two-photon quantum walk in a multimode fiber," Sci. Adv. 2, e1501054 (2016).
   T. A. W. Wolterink, R. Uppu, G. Ctistis, W. L. Vos, K.-J. Boller, and P. W. H. Pinkse, "Programmable two-photon quantum interference in 10<sup>3</sup> channels in opaque scattering media," Phys. Rev. A 93, 053817 (2016).
- <sup>25</sup> H. Defienne, M. Reichert, and J. W. Fleischer, "Adaptive quantum optics with spatially entangled photon pairs," Phys. Rev. Lett. **121**, 233601 (2018).
- <sup>26</sup>Y. Peng, Y. Qiao, T. Xiang, and X. Chen, "Manipulation of the spontaneous parametric down-conversion process in space and frequency domains via wavefront shaping," Opt. Lett. **43**, 3985–3988 (2018).
- <sup>27</sup>O. Lib, G. Hasson, and Y. Bromberg, "Real-time shaping of entangled photons by classical control and feedback," Sci. Adv. 6, eabb6298 (2020).
- <sup>28</sup>O. Lib and Y. Bromberg, "Pump-shaping of non-collinear and non-degenerate entangled photons," Opt. Lett. **45**, 6827–6830 (2020).
- <sup>29</sup>G. Soro, E. Lantz, A. Mosset, and F. Devaux, "Quantum spatial correlations imaging through thick scattering media: Experiments and comparison with simulations of the biphoton wave function," J. Opt. 23, 025201 (2021).
- <sup>30</sup>P. Cameron, B. Courme, C. Vernière, R. Pandya, D. Faccio, and H. Defienne, "Adaptive optical imaging with entangled photons," Science 383, 1142–1148 (2024).
- <sup>31</sup> R. Shekel, O. Lib, and Y. Bromberg, "Shaping entangled photons through arbitrary scattering media using an advanced wave beacon," Opt. Quantum **2**, 303–309 (2024).
- <sup>32</sup>B. Courme, C. Vernière, M. Joly, D. Faccio, S. Gigan, and H. Defienne, "Non-classical optimization through complex media," arXiv:2503.24283 (2025).

- <sup>33</sup> K. Bajar, R. Shekel, V. S. Bhat, R. Chatterjee, Y. Bromberg, and S. Mujumdar, "Rapid and efficient wavefront correction for spatially entangled photons using symmetrized optimization," arXiv:2504.19490 (2025).
- <sup>34</sup>R. Shekel, O. Lib, A. Sardas, and Y. Bromberg, "Shaping entangled photons through emulated turbulent atmosphere," OSA Continuum 4, 2339–2350 (2021).
   <sup>35</sup>I. M. Vellekoop and A. P. Mosk, "Phase control algorithms for focusing light through turbid media," Opt. Commun. 281, 3071–3080 (2008).
- <sup>36</sup>S. P. Walborn, C. H. Monken, S. Pádua, and P. H. Souto Ribeiro, "Spatial correlations in parametric down-conversion," Phys. Rep. 495, 87–139 (2010).
- <sup>37</sup>J. C. Howell, R. S. Bennink, S. J. Bentley, and R. W. Boyd, "Realization of the Einstein-Podolsky-Rosen paradox using momentum- and position-entangled photons from spontaneous parametric down conversion," Phys. Rev. Lett. **92**, 210403 (2004).
- <sup>38</sup>E. Akkermans and G. Montambaux, *Mesoscopic Physics of Electrons and Photons* (Cambridge University Press, 2007).
- <sup>39</sup> J. W. Goodman, *Speckle Phenomena in Optics: Theory and Applications* (Roberts and Company Publishers, 2007).
- <sup>40</sup>A. Goetschy and A. D. Stone, "Filtering random matrices: The effect of incomplete channel control in multiple scattering," Phys. Rev. Lett. 111, 063901 (2013).
- <sup>41</sup>D. N. Klyshko, "A simple method of preparing pure states of an optical field, of implementing the Einstein-Podolsky-Rosen experiment, and of demonstrating the complementarity principle," Sov. Phys. Usp. 31, 74 (1988).
- <sup>42</sup>A. Belinskii and D. Klyshko, "Two-photon optics: Diffraction, holography, and transformation of two-dimensional signals," Sov. J. Exp. Theor. Phys. **78**, 259–262 (1994).
- <sup>43</sup>Y. Zheng, J.-S. Xu, C.-F. Li, and G.-C. Guo, "Theory of monochromatic advanced-wave picture and applications in biphoton optics," arXiv:2412.02088 [quant-ph] (2024).
- <sup>44</sup>M. Cui and C. Yang, "Implementation of a digital optical phase conjugation system and its application to study the robustness of turbidity suppression by phase conjugation," Opt. Express 18, 3444–3455 (2010).
- <sup>45</sup>R. W. Boyd, A. L. Gaeta, and E. Giese, "Nonlinear optics," in *Springer Handbook of Atomic, Molecular, and Optical Physics* (Springer, 2008), pp. 1097–1110.
- <sup>46</sup>S. Arora, E. Berger, H. Elad, G. Kindler, and M. Safra, "On non-approximability for quadratic programs," in *46th Annual IEEE Symposium on Foundations of Computer Science (FOCS'05)* (IEEE, 2005), pp. 206–215.
- <sup>47</sup>P. M. Pardalos and S. A. Vavasis, "Quadratic programming with one negative eigenvalue is NP-hard," J. Glob. Optim. 1, 15–22 (1991).
- <sup>48</sup> A. Lucas, "Ising formulations of many np problems," Front. Phys. **2**, 5 (2014).
- <sup>49</sup>D. Pierangeli, G. Marcucci, and C. Conti, "Large-scale photonic Ising machine by spatial light modulation," Phys. Rev. Lett. **122**, 213902 (2019).
- <sup>50</sup> D. Pierangeli, M. Rafayelyan, C. Conti, and S. Gigan, "Scalable spin-glass optical simulator," Phys. Rev. Appl. 15, 034087 (2021).
- <sup>51</sup> A. Al-Sulami, H. Fawzi, and S. Sun, "Exact algorithms for quadratic optimization over roots of unity," arXiv:2508.02006 (2025).
- <sup>52</sup>R. Shekel (2025). "Code and data for publication: 'Fundamental bounds of wavefront shaping of spatially entangled photons," Zenodo. https://doi.org/10.5281/zenodo.17036996
- <sup>53</sup>R. Carminati and J. C. Schotland, *Principles of Scattering and Transport of Light* (Cambridge University Press, 2021).
- 54 O. Lib and Y. Bromberg, "Thermal biphotons," APL Photonics 7, 031301 (2022).
- <sup>55</sup>C. H. Monken, P. H. S. Ribeiro, and S. Pádua, "Transfer of angular spectrum and image formation in spontaneous parametric down-conversion," Phys. Rev. A 57, 3123 (1998).
- <sup>56</sup>C. K. Law and J. H. Eberly, "Analysis and interpretation of high transverse entanglement in optical parametric down conversion," Phys. Rev. Lett. **92**, 127903 (2004).
- <sup>57</sup>M. P. van Exter, A. Aiello, S. S. R. Oemrawsingh, G. Nienhuis, and J. P. Woerdman, "Effect of spatial filtering on the Schmidt decomposition of entangled photons," Phys. Rev. A 74, 012309 (2006).
- <sup>58</sup>B. Mastiani, D. W. S. Cox, and I. M. Vellekoop, "Practical considerations for high-fidelity wavefront shaping experiments," J. Phys.: Photonics **6**, 033003 (2024).

- <sup>59</sup> H. Di Lorenzo Pires, J. Woudenberg, and M. P. van Exter, "Statistical properties of two-photon speckles," Phys. Rev. A 85, 033807 (2012).
- <sup>60</sup> F. Scheffold and G. Maret, "Universal conductance fluctuations of light," Phys. Rev. Lett. 81, 5800 (1998).
- <sup>61</sup>S. Leedumrongwatthanakun, L. Innocenti, H. Defienne, T. Juffmann, A. Ferraro, M. Paternostro, and S. Gigan, "Programmable linear quantum networks with a multimode fibre," Nat. Photonics **14**, 139–142 (2020).
- <sup>62</sup>S. Goel, S. Leedumrongwatthanakun, N. H. Valencia, W. McCutcheon, A. Tavakoli, C. Conti, P. W. Pinkse, and M. Malik, "Inverse design of high-dimensional quantum optical circuits in a complex medium," Nat. Phys. 20, 232–239 (2024).
- <sup>63</sup> N. H. Valencia, S. Goel, A. Ma, S. Leedumrongwatthanakun, F. Graffitti, A. Fedrizzi, W. McCutcheon, and M. Malik, "A multiplexed programmable quantum photonic network," in *Quantum 2.0* (Optica Publishing Group, 2024), p. QTh2B–6.
- p. QTh2B-6. <sup>64</sup>Y. Lahini, Y. Bromberg, D. N. Christodoulides, and Y. Silberberg, "Quantum correlations in two-particle Anderson localization," Phys. Rev. Lett. **105**, 163905 (2010).

- <sup>65</sup>A. N. Black, E. Giese, B. Braverman, N. Zollo, S. M. Barnett, and R. W. Boyd, "Quantum nonlocal aberration cancellation," Phys. Rev. Lett. 123, 143603 (2019).
- <sup>66</sup>M. Safadi, O. Lib, H.-C. Lin, C. W. Hsu, A. Goetschy, and Y. Bromberg, "Coherent backscattering of entangled photon pairs," Nat. Phys. **19**, 562–568 (2023).
- <sup>67</sup> K. Bajar, R. Chatterjee, V. S. Bhat, and S. Mujumdar, "Partial immunity of two-photon correlation against wavefront distortion for spatially entangled photons," APL Quantum 2, 016105 (2025).
- <sup>68</sup>S. Monin, M. Alterman, and A. Levin, "Rapid wavefront shaping using an optical gradient acquisition," arXiv:2501.13711 (2025).
- $^{69}$  P. del Hougne and G. Lerosey, "Leveraging chaos for wave-based analog computation: Demonstration with indoor wireless communication signals," Phys. Rev. X **8**, 041037 (2018).
- <sup>70</sup>F. Xia, K. Kim, Y. Eliezer, S. Han, L. Shaughnessy, S. Gigan, and H. Cao, "Nonlinear optical encoding enabled by recurrent linear scattering," Nat. Photonics **18**, 1067–1075 (2024).
- <sup>71</sup> M. Yildirim, N. U. Dinc, I. Oguz, D. Psaltis, and C. Moser, "Nonlinear processing with linear optics," Nat. Photonics 18, 1076–1082 (2024).